APPLIED AND ENVIRONMENTAL MICROBIOLOGY, Nov. 2007, p. 7427–7434 Vol. 73, No. 22
0099-2240/07/$08.00+0 doi:10.1128/AEM.01101-07

Sequential Aldol Condensation Catalyzed by Hyperthermophilic 2-Deoxy-D-Ribose-5-Phosphate Aldolase▽†

Haruhiko Sakuraba,[1] Kazunari Yoneda,[1] Kumiko Yoshihara,[1] Kyoko Satoh,[1] Ryushi Kawakami,[2] Yoshihiro Uto,[1] Hideaki Tsuge,[3] Katsuyuki Takahashi,[4] Hitoshi Hori,[1] and Toshihisa Ohshima[5]*

Department of Life System, Institute of Technology and Science, University of Tokushima, 2-1 Minamijosanjima-cho, Tokushima 770-8506, Japan[1]; Analytical Research Center for Experimental Sciences, Saga University, 1 Honjo-machi, Saga 840-8502, Japan[2]; Institute for Health Science, Tokushima Bunri University, Yamashiro-cho, Tokushima 770-8514, Japan[3]; Catalysis Science Laboratory, Mitsui Chemicals, Inc., 1144, Togo, Mobara-shi, Chiba 297-0017, Japan[4]; and Microbial Genetics Division, Institute of Genetic Resources, Faculty of Agriculture, Kyushu University, 6-10-1 Hakozaki, Higashi-ku, Fukuoka 812-8581, Japan[5]

Received 17 May 2007/Accepted 15 September 2007

Genes encoding 2-deoxy-D-ribose-5-phosphate aldolase (DERA) homologues from two hyperthermophiles, the archaeon *Pyrobaculum aerophilum* and the bacterium *Thermotoga maritima*, were expressed individually in *Escherichia coli*, after which the structures and activities of the enzymes produced were characterized and compared with those of *E. coli* DERA. To our surprise, the two hyperthermophilic DERAs showed much greater catalysis of sequential aldol condensation using three acetaldehydes as substrates than the *E. coli* enzyme, even at a low temperature (25°C), although both enzymes showed much less 2-deoxy-D-ribose-5-phosphate synthetic activity. Both the enzymes were highly resistant to high concentrations of acetaldehyde and retained about 50% of their initial activities after a 20-h exposure to 300 mM acetaldehyde at 25°C, whereas the *E. coli* DERA was almost completely inactivated after a 2-h exposure under the same conditions. The structure of the *P. aerophilum* DERA was determined by X-ray crystallography to a resolution of 2.0 Å. The main chain coordinate of the *P. aerophilum* enzyme monomer was quite similar to those of the *T. maritima* and *E. coli* enzymes, whose crystal structures have already been solved. However, the quaternary structure of the hyperthermophilic enzymes was totally different from that of the *E. coli* DERA. The areas of the subunit-subunit interface in the dimer of the hyperthermophilic enzymes are much larger than that of the *E. coli* enzyme. This promotes the formation of the unique dimeric structure and strengthens the hydrophobic intersubunit interactions. These structural features are considered responsible for the extremely high stability of the hyperthermophilic DERAs.

Using acetaldehyde and D-glyceraldehyde-3-phosphate as substrates, 2-deoxy-D-ribose-5-phosphate aldolase (DERA; EC 4.1.2.4) catalyzes a reversible aldol reaction that generates 2-deoxy-D-ribose-5-phosphate (DRP) (1, 17). DERA is unique in that it catalyzes the aldol reaction between two aldehydes, which serve as both the aldol donor and the acceptor components. In addition, DERA is the only aldolase known to accept three aldehydes in a sequential and stereoselective manner during an aldol condensation reaction, which makes it a particularly interesting potential biocatalyst for synthetic organic chemistry. Gijsen and Wong (6) were the first to observe *Escherichia coli* DERA ($DERA_{Eco}$) catalyze a double aldol condensation of three acetaldehyde molecules (Fig. 1): the reaction started with a stereospecific addition of acetaldehyde to a substituted acetaldehyde to form 3-hydroxy-4-substituted butylaldehyde, which in turn reacted with a third acetaldehyde. After the second condensation, the product (compound 1) largely cyclized to form stable 2,4,6-trideoxy-D-erythro-hexapyranoside, which is a useful chiral synthon of hydroxymethylglutaryl-coenzyme A reductase inhibitors. This has prompted investigation of the feasibility of applying $DERA_{Eco}$ for the synthesis of cholesterol-lowering agents (5–7, 23). The practical application of this enzyme, however, is still limited by its poor resistance to an aldehyde concentration that is high enough to be useful for biocatalysis (11).

Recently, much attention has been paid to the isolation and characterization of enzymes from hyperthermophiles because of their great potential to serve as a new source of enzymes that are much more stable than their counterparts from mesophiles. DERAs from only two hyperthermophiles, *Aeropyrum pernix* (19) and *Thermococcus kodakaraensis* (18), have been studied. Both of the enzymes are very stable and could potentially serve as synthetic catalysts, although only their ability to catalyze cleavage of DRP has been characterized, thus far. Aldol condensation catalyzed by hyperthermophilic DERA homologues remains unclear.

In the present study, DERAs from two hyperthermophiles, the archaeon *Pyrobaculum aerophilum* and the bacterium *Thermotoga maritima*, were compared with $DERA_{Eco}$ in terms of their capacity to catalyze aldol condensation. We found that both enzymes are highly resistant to acetaldehyde and exhibit much greater catalysis of sequential aldol condensation of

* Corresponding author. Mailing address: Microbial Genetics Division, Institute of Genetic Resources, Faculty of Agriculture, Kyushu University, 6-10-1 Hakozaki, Higashi-ku, Fukuoka 812-8581, Japan. Phone: 81 92 642 3053. Fax: 81 92 642 3059. E-mail: ohshima@agr.kyushu-u.ac.jp.

† Supplemental material for this article may be found at http://aem.asm.org/.

▽ Published ahead of print on 28 September 2007.

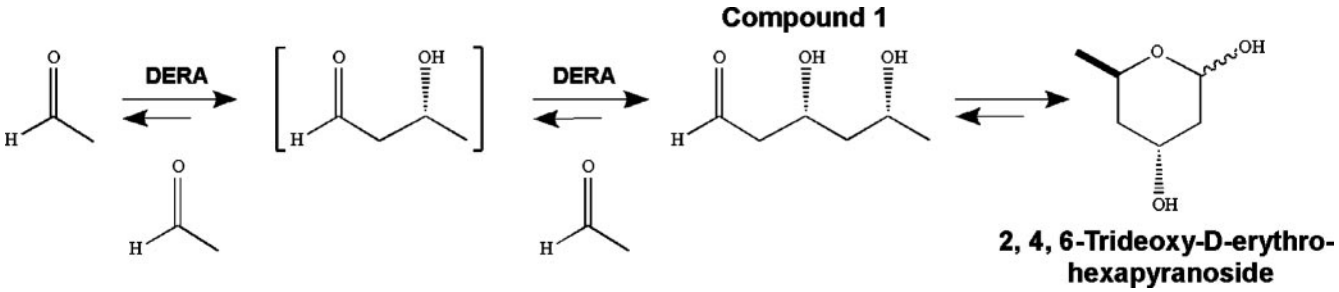

FIG. 1. Sequential aldol condensations catalyzed by DERA. (Reprinted with permission from reference 6. Copyright 1994, American Chemical Society.)

three acetaldehydes than the *E. coli* enzyme, even at room temperature (25°C). The structure of the $DERA_{Eco}$ has already been reported by Heine et al. (8, 9), and that of the *T. maritima* DERA ($DERA_{Tma}$) is available in the Protein Data Bank. We therefore also determined the crystal structure of the *P. aerophilum* DERA ($DERA_{Pae}$) and then compared the architectures of the three enzymes and evaluated the structural features responsible for the extremely high stability of the hyperthermophilic enzymes and their robust propulsive force of sequential aldol condensation.

MATERIALS AND METHODS

Materials. The pET-11a vector was obtained from Novagen (Madison, WI). The *E. coli* strain BL21-CodonPlus-RIL(DE3) was purchased from Stratagene (La Jolla, CA). DRP, triose-phosphate isomerase, and glycerol-3-phosphate dehydrogenase were purchased from Sigma (St. Louis, MO). Restriction enzymes were purchased from New England Biolabs, Inc. (Beverly, MA). All other chemicals were of reagent grade.

Cloning, protein expression, and purification. The genes encoding $DERA_{Tma}$ (open reading frame TM1559) and $DERA_{Pae}$ (open reading frame PAE1231) were amplified by PCR (the gene information is available at www.genome.jp/kegg) using the following sets of oligonucleotide primers: 5′-TATATCATATG ATAGAGTACAGGATTGAG-3′ and 5′-TTATGGATCCCTCAAC CTCCAT ATCTCTC-3′ for $DERA_{Tma}$ and 5′-GCGGCCATATGATACATTTAGTA GA CTACG-3′ and 5′-TAATGGATCCCTATAGAAGAGCCTCTGGGG-3′ for $DERA_{Pae}$. In each case, the forward primer introduced a unique NdeI restriction site that overlapped the 5′ initiation codon, while the reverse primer introduced a unique BamHI restriction site proximal to the 3′ end of the termination codon. Chromosomal DNA isolated as described previously (20) was used as the template. The amplified fragments were digested with NdeI and BamHI and ligated into the expression vector pET11a (Novagen) linearized with NdeI and BamHI, yielding pPAE for $DERA_{Pae}$ and pTMA for $DERA_{Tma}$.

To prepare recombinant $DERA_{Pae}$, the *E. coli* strain BL21(DE3) codon plus RIL (Stratagene) was transformed with pPAE, after which the transformants were cultivated at 37°C in a medium containing 12 g of tryptone, 24 g of yeast extract, 5 ml of glycerol, 12.5 g of K_2HPO_4, 3.8 g of KH_2PO_4, and 50 mg of ampicillin/liter until the optical density at 600 nm reached 0.6. Expression was induced by adding 1 mM isopropyl-β-D-thiogalactopyranoside to the medium, and cultivation was continued for an additional 3 h at 37°C. The cells were then harvested by centrifugation, suspended in 10 mM Tris-HCl buffer (pH 8.0) and disrupted by sonication. After the lysate was centrifuged (15,000 × *g* for 20 min), the supernatant was heated for 20 min at 90°C and then clarified by centrifugation. This supernatant was then subjected to gel filtration on a Superdex 200 26/60 column (GE Healthcare) equilibrated with 10 mM Tris-HCl buffer (pH 8.0) containing 0.2 M NaCl, after which the resulting protein solution was dialyzed against 10 mM Tris-HCl buffer (pH 8.0). Preparation of the recombinant $DERA_{Tma}$ was carried out using the same procedure, except pTMA was used as the expression plasmid.

The expression vector carrying $DERA_{Eco}$ (the pECO:$DERA_{Eco}$ gene was amplified by PCR and inserted into the EcoRI-HindIII site of pUC18) was kindly provided by Catalysis Science Laboratory, Mitsui Chemicals, Inc. (Chiba, Japan), and *E. coli* cells transformed with pECO were cultivated as described above. After disrupting the cells by sonication, the cell debris was removed by centrifugation, and nucleic acids were removed by addition of streptomycin sulfate to a final concentration of 1%, followed by centrifugation. The resultant supernatant was loaded onto a DEAE-Toyopearl column (Tosoh, Tokyo, Japan) equilibrated with 10 mM Tris-HCl buffer (pH 8.0). After the column was washed with the same buffer, the enzyme was eluted with a linear gradient of 0 to 0.2 M NaCl in the same buffer. The active fractions were pooled, $(NH_4)_2SO_4$ was added to the solution to 40% saturation, and the resulting solution was placed on a butyl-Toyopearl column (Tosoh) equilibrated with 10 mM Tris-HCl buffer (pH 8.0) supplemented with 40% $(NH_4)_2SO_4$. After the column was washed with the same buffer, the enzyme was eluted with a linear gradient of 40 to 0% $(NH_4)_2SO_4$ in the same buffer. The active fractions were collected, and the solution was subjected to gel filtration with a Superdex 200 26/60 column, as described above. The resulting protein solution was then dialyzed against 10 mM Tris-HCl buffer (pH 8.0).

Enzyme assay and determination of protein concentration. Assays for the DRP cleavage and aldol condensation were carried out at 25°C, due to the lability of aldehydes at higher temperatures. The DRP cleavage activity was determined by measuring the oxidation of NADH in a coupled assay using triose-phosphate isomerase and glycerol-3-phosphate dehydrogenase. The assay mixture contained 100 mM buffer, 0.1 mM NADH, 0.4 mM DRP, 11 units of triose-phosphate isomerase (rabbit muscle), 4 units of glycerol-3-phosphate dehydrogenase (rabbit muscle), and the DERA preparation in a total volume of 1.00 ml. Imidazole-HCl (pH 6.5), sodium acetate (pH 6.0), and triethanolamine-HCl (pH 7.5) were used as the buffer for $DERA_{Tma}$, $DERA_{Pae}$, and $DERA_{Eco}$, respectively. The change in absorbance of NADH was followed at 340 nm (ε = 6.22 mM^{-1} cm^{-1}). The Michaelis constants were determined with the nonlinear regression analysis of the data obtained from the initial rate of D-glyceraldehyde-3-phosphate formation at 25°C by using an enzyme kinetics module of SigmaPlot (Hulinks, Inc., Tokyo, Japan).

The protein concentration was determined using the Bradford method (2), with a standard assay kit from Bio-Rad (Hercules, CA); bovine serum albumin served as the standard.

The aldol condensation reaction was analyzed using thin-layer chromatography (TLC) with catalog code PE-SIL-G/UV (Whatman, United Kingdom) TLC plates. The assay mixture for DRP production contained 100 mM buffer, 300 mM acetaldehyde, 50 mM glyceraldehyde-3-phosphate, and the DERA preparation (0.5 μg) in a total volume of 50 μl. For the sequential aldol reaction mixture, glyceraldehyde-3-phosphate was omitted from the assay mixture, and 23 μg of enzyme was used. Sodium acetate (pH 5.5), sodium acetate (pH 6.0), and imidazole-HCl (pH 6.5) were used as the buffer for the DRP synthesis of $DERA_{Pae}$, $DERA_{Tma}$, and $DERA_{Eco}$, respectively. On the other hand, sodium acetate (pH 6.0), imidazole-HCl (pH 6.0), and imidazole-HCl (pH 7.0) were used as the buffer for the sequential aldol reaction of $DERA_{Pae}$, $DERA_{Tma}$, and $DERA_{Eco}$, respectively. After incubation for an appropriate time at 25°C, the reaction was stopped by cooling on ice. Each solution was then passed through a centrifugal filter device (Microcon YM-30; Millipore, Tokyo, Japan) to remove protein, and an aliquot (2 μl) of the filtrate was subjected to TLC analysis. The developing systems for DRP and 2,4,6-trideoxy-D-erythro-hexapyranoside consisted of 1-butanol, acetic acid, and H_2O at ratios of 4:2:3 (vol/vol/vol) and 4:1:1 (vol/vol/vol), respectively. The spots of the reaction products were localized with anisaldehyde reagent (5% [vol/vol] anisaldehyde, and 10% [vol/vol] H_2SO_4 in methanol).

The products of the sequential aldol reaction with acetaldehyde were analyzed by ^1H nuclear magnetic resonance (NMR). The reaction system was similar to that described above, except the reaction mixture utilized 23 mg of enzyme in a 50-ml volume. The mixture was then stirred in the dark for 2 days at 25°C, after which the solution was passed through a centrifugal filter device (Amicon Ultra

PL-30; Millipore). The filtrate was then lyophilized and further purified through two silica gel chromatography steps using dichloromethane-methanol (10:1) and ethyl acetate. ^{1}H NMR spectra were recorded on a JEOL JMS-AX500 spectrometer (400 MHz) using tetramethylsilane as the internal standard. Mass spectra were measured on a JEOL JMS-DX-303 mass spectrometer using the electron ionization method.

Stability and pH optimum. To examine the effects of acetaldehyde on enzyme stability, the enzyme preparations in 10 mM Tris-HCl buffer (0.5 mg/ml; pH 8.0) containing 300 mM acetaldehyde were incubated at 25°C, after which the residual activity was determined at appropriate intervals by using the assay for DRP cleavage. Prior to analysis of the enzyme activity, the acetaldehyde was removed from the enzyme solution by using a centrifugal filter device (Microcon YM-10; Millipore); the sample was concentrated and then diluted to the original volume with 10 mM Tris-HCl buffer (pH 8.0), and the cycle was repeated. To assess thermostability, the enzyme (0.5 mg/ml) was incubated for 10 min at different temperatures, after which the residual activities were assayed. To determine pH stability, the enzyme (0.5 mg/ml) was incubated for 30 min at 50°C in buffers of different pHs, after which the remaining activities were assayed. The buffers (500 mM) used were sodium acetate, potassium phosphate, Tris-HCl, glycine-NaOH, and Na_2HPO_3-NaOH for pH ranges of 3.5 to 6.0, 6.0 to 7.5, 7.5 to 8.5, 8.5 to 11.0, and 11.0 to 12.5, respectively. The buffers used to determine the optimal pH of the enzyme were sodium acetate (0.1 M), imidazole-HCl (0.1 M), triethanolamine-HCl (0.1 M), and glycine-NaOH (0.1 M) for pH ranges of 5.0 to 6.0, 6.0 to 7.5, 7.5 to 8.5, and 8.5 to 11.0, respectively. The DRP cleavage assay was used.

The optimal pH for the aldol condensation was determined using TLC analysis. After localization of the product spots, the TLC plate was scanned, and the relative ratios of the peak areas were determined using ImageJ software (rsb.info.nih.gov/ij/).

Crystallization and data collection. Crystallization conditions were screened using Wizard 1 and 2 (Emerald Biostructure). Crystals of $DERA_{Pae}$ were obtained using the hanging drop vapor diffusion method, in which 2 μl of 14 mg/ml protein was mixed with an equal volume of mother liquor, which consisted of 20% (wt/vol) polyethylene glycol 1000, 0.2 M zinc acetate, and 0.1 M acetate buffer (pH 4.5). The crystals were grown at 20°C for 3 days and were found to belong to the hexagonal space group $P6_3$, with unit cell parameters of a = b = 84.5 Å and c = 112.6 Å, and to diffract to 2.0 Å. We collected the diffraction data on an R-AXIS VII imaging plate detector using a rotating copper anode in-house generator (MicroMax007, Rigaku, Japan) operating at 40 kV and 20 mA. All measurements were carried out on crystals cryoprotected with 30% (wt/vol) trehalose and cooled to 100 K in a stream of nitrogen gas. The data were processed using HKL2000 (16).

Phasing and refinement. Heavy-atom derivatives were prepared by soaking the crystals in a reservoir solution containing 1 mM Hg-acetate or 1 mM $K_2Pt(SCN)_6$ (Hampton Research) for 7 h. Phase calculation was carried out by the multiple-isomorphous-replacement-with-an-anomalous-scattering (MIRAS) method by using SOLVE software (22). The resultant MIRAS map at 2.0 Å was subjected to maximum-likelihood density modification, followed by autotracing using RESOLVE (22). The model was built using XtalView (13), and refinement to a resolution of 2.0 Å was carried out using Refmac5 (14) and CNS (3) software. Then, after several cycles of inspection of the $2F_o$-F_c and F_o-F_c density maps were carried out, the model was rebuilt. The R_{cryst} and R_{free} values of the final model were 20.6% and 24.1%, respectively (Table 1). The final structure exhibited good geometry without Ramachandran outliers. Molecular graphics figures were created using PyMOL (pymol.sourceforge.net/).

Protein structure accession numbers. The atomic coordinates and structure factors (code 1VCV) have been deposited in the Protein Data Bank, Research Collaboratory for Structural Bioinformatics, Osaka University, Japan (www.rcsb.org/).

TABLE 1. X-ray data collection and refinement statistics

Data collection	Native	Derivative data	
		Hg-acetate	$K_2Pt(SCN)_6$
Space group	$P6_3$		
Unit-cell parameters (Å)	a = b = 84.5, c = 112.6		
Maximum resolution (Å)	2.0	2.0	2.0
No. of unique reflections	30105	59423	58695
Redundancy	7.5	3.6	3.8
Completeness (%)[a]	97.3 (91.7)	97.2 (91.7)	96.7 (91.5)
R_{sym} (%)[a,b]	6.8 (21.6)	6.5 (27.3)	4.8 (20.1)
<*I*/*Sigma I*>[c]	9.8	8.9	10.3
Wilson B-factor (Å^2)[d]	21.8	25.2	24.1
Phasing (MIRAS)			
No. of sites		4	4
Figure of merit	0.34 (28.1–2.0 Å)		
Refinement			
Resolution range (Å)	28.1–2.0 Å		
R_{cryst} (%)[e]	20.6		
R_{free} (%)[f]	24.1		
No. of protein atoms	3461		
No. of water molecules	193		
RMSD bond length (Å)	0.005		
RMSD bond angle (°)	1.3		
Average B-factor (Å^2)	27.4		
Ramachandran statistics[g]	93.3/6.27/0/0		

[a] Numbers in parentheses refer to the respective highest resolution data shell in each data set.

[b] $R_{sym} = \dfrac{\sum_h \sum_i |I(h,i) - \langle I\rangle(h)|}{\sum_h \sum_i \langle I\rangle(h)}$ where $I(h,i)$ is the scaled intensity of the ith observation of reflection h and $\langle I\rangle(h)$ is the mean value, and the summation is the overall measurement.

[c] For the highest resolution shell, number of the reflections with *I*/*Sigma I* less than 1 was 436 (14.0%).

[d] Resolution limits used for scaling are 4.5 to 2.0 Å.

[e] $R_{cryst} = \dfrac{\sum_{h,k,l} ||F_{obs}| - k|F_{calc}||}{\sum_{h,k,l} |F_{obs}|}$, where F_{obs} and F_{calc} are the observed and calculated structure factors, respectively, k is a weighting factor, and the summation is over 95% of the reflections in the working set.

[f] $R_{free} = \dfrac{\sum_{h,k,l} ||F_{obs}| - k|F_{calc}||}{\sum_{h,k,l} |F_{obs}|}$ is the summation over 5% of the reflections chosen randomly.

[g] Ramachandran statistics indicate the fraction of residues in the most favored, the additionally allowed, the generously allowed, and the disallowed regions of the Ramachandran diagram, as defined by PROCHECK (12).

RESULTS

Comparison of DRP cleavage reaction and thermal/pH stability. The optimal pH levels for DRP cleavage catalyzed by the purified enzymes were around 6.0, 6.5, and 7.5 for $DERA_{Pae}$, $DERA_{Tma}$ and $DERA_{Eco}$, respectively (Fig. 2A). The specific activities of $DERA_{Pae}$ (0.25 ± 0.03 μmol/min/mg) and $DERA_{Tma}$ (1.00 ± 0.07 μmol/min/mg) for DRP cleavage were substantially lower than that of $DERA_{Eco}$ (58 ± 2 μmol/min/mg) at 25°C. All three enzymes exhibited typical Michaelis-Menten kinetics at 25°C, and the apparent K_m values for DRP were calculated as 0.066 ± 0.004, 0.020 ± 0.003, and 0.23 ± 0.01 mM for $DERA_{Pae}$, $DERA_{Tma}$, and $DERA_{Eco}$, respectively. Both $DERA_{Pae}$ and $DERA_{Tma}$ retained full activity when heated for 10 min at 90°C. At 100°C, however, the activity of $DERA_{Tma}$ was almost completely lost, while that of $DERA_{Pae}$ was largely unchanged (Fig. 2B), indicating the greater stability of $DERA_{Pae}$ at that temperature. On the other hand, $DERA_{Eco}$ was largely inactivated by incubation at temperatures of >60°C (Fig. 2B). Both hyperthermophilic enzymes were extremely stable over a wide range of pH levels: when they were heated for 30 min at 50°C, they showed no loss of activity at pH levels ranging from 5.0 to 11.0, while $DREA_{Eco}$ showed significant loss of activity at pH levels of more than 10.0 and less than 5.5 (Fig. 2C).

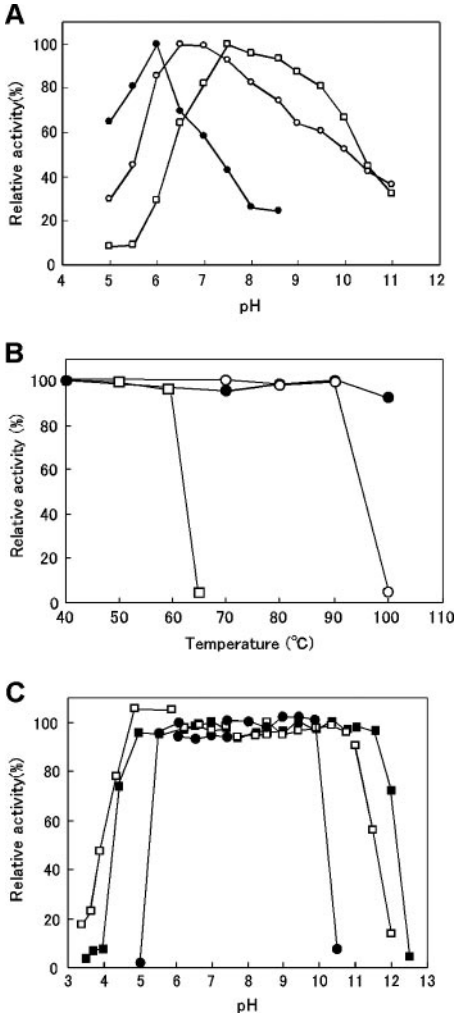

FIG. 2. Optimal pH levels for DRP cleavage and thermal/pH stability. (A) The DRP cleavage assay was performed at various pH levels at 25°C. Filled circles, $DERA_{Pae}$; open circles, $DERA_{Tma}$; open squares, $DERA_{Eco}$. (B) After incubation for 10 min at the indicated temperatures, the remaining activity was assayed. Filled circles, $DERA_{Pae}$; open circles, $DERA_{Tma}$; open squares, $DERA_{Eco}$. (C) The enzyme was incubated for 30 min at 50°C in buffers of various pH levels, after which the remaining activity was assayed. Filled squares, $DERA_{Pae}$; open squares, $DERA_{Tma}$; filled circles, $DERA_{Eco}$.

Comparison of aldol condensation reaction. The optimal pH levels for DRP synthesis were estimated to be around 5.5 (sodium acetate buffer), 6.0 (sodium acetate buffer), and 6.5 (imidazole-HCl buffer) for $DERA_{Pae}$, $DERA_{Tma}$, and $DERA_{Eco}$, respectively, while those for the sequential aldol reaction were 6.0 (sodium acetate buffer), 6.0 (imidazole-HCl buffer), and 7.0 (imidazole-HCl buffer) for $DERA_{Pae}$, $DERA_{Tma}$, and $DERA_{Eco}$, respectively. In addition, we found that after the reaction was run for 2 h at 25°C, a comparatively large amount of DRP was produced with $DERA_{Eco}$, but only a small amount was produced with $DERA_{Tma}$ or $DERA_{Pae}$ (Fig. 3A).

By contrast, in the sequential aldol condensation with acetaldehyde (for 20 h at 25°C), unexpectedly large amounts of the product were observed with the hyperthermophilic enzymes (Fig. 3B), whereas only a trace of the product was obtained

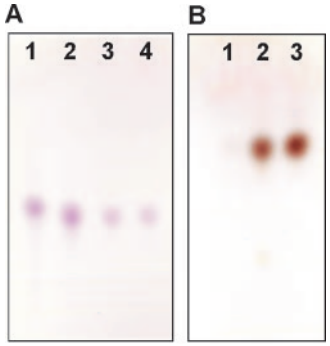

FIG. 3. TLC analysis of the products by aldol condensation. (A) DRP synthesis. Lane 1, DRP standard; lane 2, reaction mixture with $DERA_{Eco}$; lane 3, reaction mixture with $DERA_{Pae}$; lane 4, reaction mixture with $DERA_{Tma}$. (B) Sequential aldol reaction with acetaldehyde. Lane 1, reaction mixture with $DERA_{Eco}$; lane 2, reaction mixture with $DERA_{Pae}$; lane 3, reaction mixture with $DERA_{Tma}$. The product was identified as 2,4,6-trideoxy-D-erythro-hexapyranoside, using ^1H NMR, as described in Materials and Methods.

with $DERA_{Eco}$ under the same conditions. A comparison of the physical properties of our product with those previously described for the $DERA_{Eco}$ product (6) enabled us to identify it as 2,4,6-trideoxy-D-erythro-hexapyranoside (see Fig. S1 in the supplemental material).

Effects of acetaldehyde on enzyme stability. Both of the hyperthermophilic DERAs were highly resistant to acetaldehyde. The $DERA_{Pae}$ and $DERA_{Tma}$ retained 53% and 46% of their DRP cleavage activity, respectively, after exposure for 20 h to 300 mM acetaldehyde at 25°C (Fig. 4). On the other hand, the $DERA_{Eco}$ is almost completely inactivated after exposure for 2 h under the same conditions (Fig. 4). Although the concentration of acetaldehyde in the hyperthermophilic DERA's reactions after 20 h is likely much less than 300 mM because of large amount of catalysis occurring with this substrate, a noteworthy difference was observed in stability between the two hyperthermophilic proteins and the mesophilic ortholog.

Architecture of $DERA_{Pae}$. The structure of $DERA_{Pae}$ was determined using the MIRAS method and refined at a 2.0-Å resolution to an R_{cryst} (R_{free}) of 20.6% (24.1%) (Table 1). Each subunit was found to be composed of 226 residues, and the

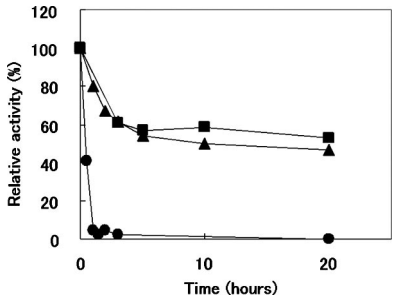

FIG. 4. Effects of acetaldehyde on enzyme stability. The enzyme was incubated at 25°C in the presence of 300 mM acetaldehyde, and the DRP cleavage activity was assayed at appropriate intervals. Filled circles, $DERA_{Eco}$. Filled squares, $DERA_{Pae}$; filled triangles, $DERA_{Tma}$.

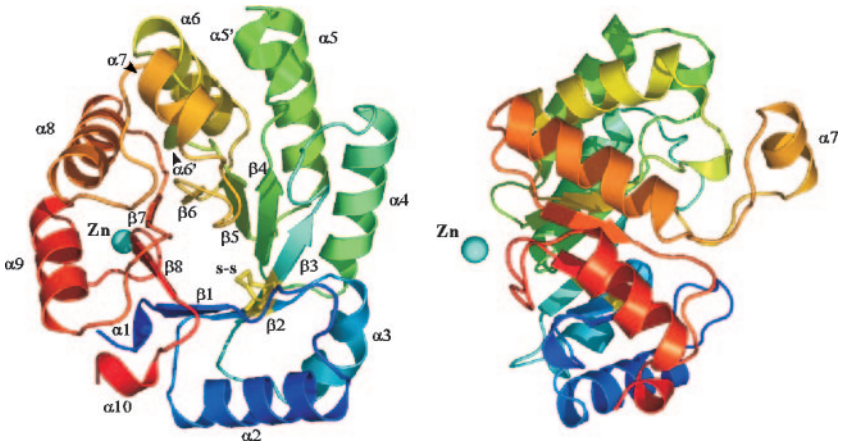

FIG. 5. Overall structure of the $DERA_{Pae}$ monomer. The multicolored drawing shows the N terminus in blue and the C terminus in red. The α helices and β strands are numbered from the N terminus. The zinc ion (Zn) is shown in light blue.

asymmetric unit consisted of two homologous subunits. The present model contained 226 ordered amino acid residues for each subunit and 193 water molecules. The subunit folded into an $(\alpha/\beta)_8$-barrel carrying two additional helical segments (Fig. 5) in which α1 helix precedes the first β strand, while α7 helix protrudes away from the barrel. The strong density of a metal ion was observed near the side chains of Asp211 and His3*. Because the crystals were obtained with mother liquor containing zinc acetate, we modeled the density as a zinc ion. Within the crystal structure, we also found one disulfide bond formed between Cys35 (β2) and Cys54 (β3) (Fig. 5).

Ion pairs and solvent-accessible surface area. Ion pair interactions within the protein structures were identified using WHAT IF Web server software (swift.cmbi.ru.nl/servers/html/index.html), with a cutoff distance of less than or equal to 4.0 Å between oppositely charged residues. The ion pairs 39, 30, and 33 were identified in the intrasubunits of $DERA_{Eco}$, $DERA_{Pae}$, and $DERA_{Tma}$, respectively. Using GRASP software (15), the total solvent-accessible surface areas (ASAs) of $DERA_{Eco}$, $DERA_{Pae}$, and $DERA_{Tma}$ monomers were determined to be 10,751, 10,046, and 11,630 $Å^2$, respectively, and their total hydrophobic areas were 2,855, 2,943, and 2,357 $Å^2$, respectively. The ASAs for the dimer interfaces in $DERA_{Pae}$ and $DERA_{Tma}$ were calculated to be 1,463 and 1,445 $Å^2$, respectively. At the interfaces, the hydrophobic interactions were observed mainly, and the hydrophobic areas were estimated to be 790 and 703 $Å^2$ for $DERA_{Pae}$ and $DERA_{Tma}$, respectively. The hydrophobic and ionic residues involved in the interactions are listed in Table 2.

DISCUSSION

$DERA_{Pae}$ and $DERA_{Tma}$ from two hyperthermophiles, the archaeon *P. aerophilum* and the bacterium *T. maritima*, were found to show thermal stability levels that were extremely higher than that of $DERA_{Eco}$. This suggests that hyperthermophilic DERAs have the potential to serve as biocatalysts in organic syntheses. Although the enzymes from the hyperthermophiles *A. pernix* (19) and *T. kodakaraensis* (18) have been reported to show similar stability levels, only their abilities to catalyze the cleavage of DRP have been characterized. In the present study, the $DERA_{Pae}$ and $DERA_{Tma}$ were compared with $DERA_{Eco}$ in terms of their capacities to catalyze aldol condensation.

Both of the hyperthermophilic enzymes showed much less DRP synthetic activity than $DERA_{Eco}$ at 25°C, as with DRP cleavage reaction. This is not surprising in view of the extremely high growth temperature (~80°C) of hyperthermophiles. By contrast, $DERA_{Tma}$ and $DERA_{Pae}$ exhibit much greater catalysis of sequential aldol condensation with three molecules of acetaldehyde than $DERA_{Eco}$, even at a low temperature. In addition, both of the enzymes were highly resistant to high concentration of acetaldehyde and retained about 50% of their initial activities after 20 h of exposure to 300 mM acetaldehyde at 25°C, whereas the $DERA_{Eco}$ is almost completely inactivated after 2 h of exposure under the same conditions. This suggests that the higher stability of the hyperthermophilic DERAs against high concentrations of acetaldehyde might lead to their higher capacity for the production of 2,4,6-trideoxy-D-erythro-hexapyranoside, though the reason for their

TABLE 2. Hydrophobic and ionic residues involved in interactions between A and B subunits

Interactions	Residues involved in the A and B subunit interactions (atom designation)	
	$DERA_{Pae}$	$DERA_{Tma}$
Hydrophobic interactions	Pro12-Phe61/Ile89 Val16-Leu91 Pro38-Leu64/Pro65 Ile39-Ala63/Leu91 Phe59-Phe61 Pro60-Pro60/Phe61 Phe61-Phe151 Leu64-Leu72	Pro42-Leu93 Phe43-Val122 Phe91-Leu93 Pro92-Pro92/Leu93 Leu93-Phe184
Ion pair interactions	Glu153 (OE1)-Lys11 (NZ) Lys11 (NZ) -Glu153 (OE1)	Glu110 OE1-Arg99 (NH1) Glu110 OE1-Arg99 (NH2) Arg99 NH1-Glu110 (OE1)

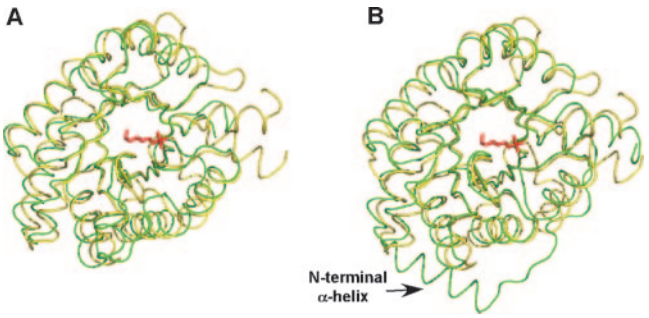

FIG. 6. Structural comparison of DERA monomers. Structures of the $DERA_{Pae}$ (A) and $DERA_{Tma}$ (B) monomers (green) superimposed on the $DERA_{Eco}$ monomer (yellow) are shown. The N-terminal α helix of $DERA_{Tma}$ is indicated by an arrow. The DRP binding site of the hyperthermophilic DERAs has been predicted based on their superposition with $DERA_{Eco}$ in complex with DRP. The DRP molecule is represented by a stick model (red).

extremely high sequential condensation activity even at a low temperature like 25°C remains to be explained.

The structure of $DERA_{Eco}$ (Protein Data Bank code 1JCL) has already been reported (8, 9), and that of $DERA_{Tma}$ (Protein Data Bank code 1O0Y) has been deposited in the Protein Data Bank by the Joint Center for Structural Genomics. As shown in Fig. 6, the main chain coordinates of the $DERA_{Pae}$ and $DERA_{Tma}$ monomers were quite similar to that of $DERA_{Eco}$. After superposition of the conserved residues within the β-barrel core, the root-mean-square deviations (RMSD) for the C-α atoms were 0.66 Å (residues Asp6, Cys35, Asp84, Lys117, Lys146, Ser148-Gly150, Lys188, Gly191-Ile193, Arg216, Gly218, and Ser220-Thr221) for $DERA_{Pae}$ and 0.47 Å (Cys65, Asp117, Lys150, Lys179-Gly183, Lys208, Gly211-Ile213, Arg229, Gly231, and Ser233-Ser234) for $DERA_{Tma}$. However, we noted three clear differences among the three enzymes: the α7 helix seen in $DERA_{Pae}$ is present in neither $DERA_{Tma}$ nor $DERA_{Eco}$; the $DERA_{Tma}$ exhibits additional 30- to 40-amino-acid sequences in the N-terminal region (including the His-tagged sequence) compared with the two other enzymes and contains an additional long arm that includes an N-terminal α helix (Fig. 6); and the $DERA_{Pae}$ contains a disulfide bond between Cys35 and Cys54 (Fig. 5). To examine the role of the disulfide bond, we prepared a C54S mutant of $DERA_{Pae}$ (data not shown). The mutant showed lower stability than the wild type, and the activity was markedly reduced when the mutant enzyme was heated for 10 min at 100°C, suggesting the positive contribution of the disulfide bond for the greater stability of $DERA_{Pae}$. The details about the mutant enzyme will be described elsewhere.

The structure of $DERA_{Eco}$ has been determined in complex with DRP (8, 9). Within that structure, the phosphate-binding pocket is composed of residues Gly171, Lys172, Gly204, Gly205, Val206, Arg207, Gly236, Ser238, and Ser239. The side chain of Ser238, the backbone amide groups of Ser238 and Gly205, and via a water molecule, the side chain of Lys172 and the backbone amide groups of Gly204, Val206, Gly171, and Ser239 all interact with the phosphate moiety of DRP (9). We predicted the DRP binding site of the hyperthermophilic DERAs based on their superposition with $DERA_{Eco}$ (Fig. 6). Most of the residues making up the phosphate-binding pocket in $DERA_{Eco}$ are conserved in both of the hyperthermophilic enzymes, except that Lys172, Val206, and Ser239 are replaced by Phe, Ile, and Thr, respectively, in $DERA_{Pae}$. In addition, Lys172 and Val206 are replaced by Phe and Ile, respectively, in $DERA_{Tma}$. These differences may account for the differences in substrate specificities of hyperthermophilic DERAs and $DERA_{Eco}$.

Recent studies of the structures of hyperthermophilic proteins have shown that the increased number of ion pairs and the enriched formation of ion pair networks are responsible mainly for the higher thermostability (10, 24). However, there are no significant differences in the numbers of total ion pairs in the intrasubunits among the three enzymes. It is thought that, in general, a smaller ASA is another feature that serves to increase protein thermostability (4). The total ASA of the $DERA_{Eco}$ monomer is similar to those of $DERA_{Pae}$ and $DERA_{Tma}$. In addition, no significant differences have been detected in the total hydrophobic areas among the three enzymes.

In solution, $DERA_{Eco}$ is reported to exist as either a monomer or a dimer (21). In a crystal form, the enzyme forms a dimeric structure with a relatively small subunit interface (Fig. 7). The ASA of the interface has been estimated to be 444 to 448 $Å^2$ (9), with a single hydrogen bond and two salt bridges present between the two subunits. Thus, the idea that the catalytic activity of this enzyme is dependent on its dimerization is not well supported by the structural evidence (9). The dimeric structure of $DERA_{Pae}$ is similar to that of $DERA_{Tma}$, but it is clearly different from that of $DERA_{Eco}$ (Fig. 7). The ASAs of the dimer interfaces in $DERA_{Pae}$ (1,463 $Å^2$) and $DERA_{Tma}$ (1,445 $Å^2$) were much larger than that of $DERA_{Eco}$. The hydrophobic interactions were observed mainly at the interfaces. The hydrophobic interaction is especially striking on the loops containing Phe59, Pro60, Phe61, and Phe151 in $DERA_{Pae}$ and on the loops containing Phe91, Pro92, Leu93, and Phe184 in $DERA_{Tma}$. These residues were buried in a large hydrophobic cluster between the two subunits in each enzyme. Only two or three salt bridges were observed between the subunits in the two enzymes (Table 2). These results suggest that an increase in intersubunit hydrophobic interactions formed by the unique dimeric structure is responsible for the extremely high stability of the two hyperthermophilic DERAs. Such interactions are not observed within the structure of $DERA_{Eco}$.

The critical residues involved in the Schiff base-mediated aldol condensation reaction in $DERA_{Eco}$ (Cys47, Asp102, Lys167, and Lys201) are completely conserved in both of the hyperthermophilic DERAs. Among these residues, the two Lys residues play a key role in the reaction mechanism of DERA. Lys167 forms a Schiff base with the substrate, whereas Lys201, which is in the proximity of the Lys167, is responsible for the perturbed pK_a of Lys167 and is involved in the stereoselective deprotonation of the donor aldehyde (8). Close to the peptide backbone of the Lys167 and Lys201 is a small hydrophobic cluster formed by Phe200, Ile166, and Met185 (Fig. 8). Though a similar hydrophobic cluster is also present in both of the hyperthermophilic enzymes, Phe200 and Met185 in $DERA_{Eco}$ are replaced by Val and Ile, respectively, in $DERA_{Pae}$, and Phe200 is replaced by Val in $DERA_{Tma}$ (Fig. 8). Recently, Jennewein et al. (11) reported that the $DERA_{Eco}$ mutant, in

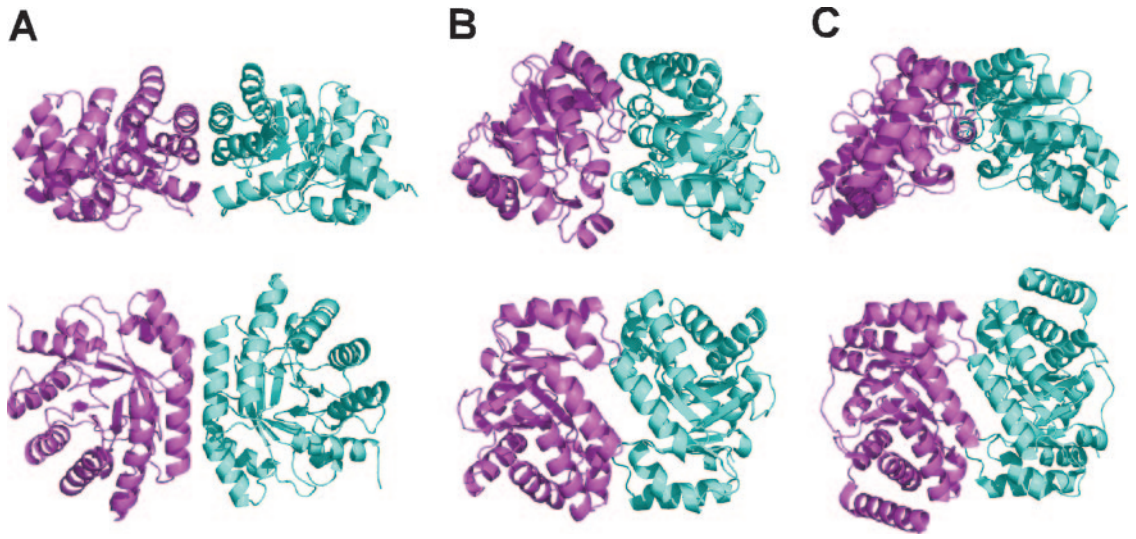

FIG. 7. Arrangement of the two DERA subunits in crystal forms. Structures of the $DERA_{Eco}$ (A), $DERA_{Pae}$ (B), and $DERA_{Tma}$ (C) dimers are shown. The lower row is the model viewed down the twofold axis.

which Phe200 was substituted for Ile, shows 14-fold improvement over the wild-type enzyme with regard to the catalysis of sequential aldol condensation of two acetaldehydes with the nonphysiological acceptor substrate chloroacetaldehyde. Since Phe200 is replaced by Val in both the hyperthermophilic DERAs, the substitution may affect the hydrophobic interaction around the scaffold of the two key Lys residues, and this might be responsible for the robust propulsive force of sequential aldol condensation by hyperthermophilic DERA homologues at low temperature. However, further study is required to elucidate the structural feature responsible for the different substrate specificities.

Practical application of $DERA_{Eco}$ has so far been limited by its instability against the substrate aldehyde (11). Clearly, the high capacities of the two hyperthermophilic DERAs as the catalyst for sequential aldol condensation at low temperature, as well as their thermal and pH stability, are strong advantages favoring practical application, and the information provided in this study may be useful for the further development of their practical application.

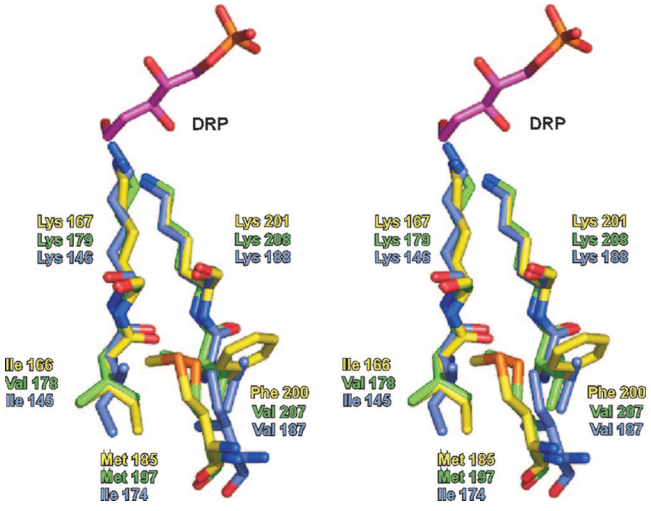

FIG. 8. Stereographic close-up of the hydrophobic cluster at the scaffold of key Lys residues. The structures of $DERA_{Pae}$ (purple) and $DERA_{Tma}$ (green) were superimposed on that of $DERA_{Eco}$ (yellow). The DRP molecule is shown as a stick model in magenta. Nitrogen, oxygen, and phosphorus atoms are shown in blue, red, and orange, respectively.

ACKNOWLEDGMENTS

This work was supported in part by a Grant-in-Aid for Scientific Research (C, no. 17613002; 2006) from the Japan Society for the Promotion of Science and the National Project on Protein Structural and Functional Analyses (Protein 3000 project) promoted by the Ministry of Education, Science, Sports, Culture, and Technology of Japan.

We thank Ikuko Shimoya-Kawakami for kind technical assistance.

REFERENCES

1. **Barbas, C. F., III, Y. F. Wang, and C. H. Wong.** 1990. Deoxyribose-5-phosphate aldolase as a synthetic catalyst. J. Am. Chem. Soc. **112:**2013–2014.
2. **Bradford, M. M.** 1976. A rapid and sensitive method for the quantitation of microgram quantities of protein utilizing the principle of protein-dye binding. Anal. Biochem. **72:**248–254.
3. **Brünger, A. T., P. D. Adams, G. M. Clore, W. L. DeLano, P. Gros, R. W. Grosse-Kunstleve, J. S. Jiang, J. Kuszewski, M. Nilges, N. S. Pannu, R. J. Read, L. M. Rice, T. Simonson, and G. L. Warren.** 1998. Crystallography & NMR system: a new software suite for macromolecular structure determination. Acta Crystallogr. D **54:**905–921.
4. **Chan, M. K., S. Mukund, A. Kletzin, M. W. Adams, and D. C. Rees.** 1995. Structure of a hyperthermophilic tungstopterin enzyme, aldehyde ferredoxin oxidoreductase. Science **267:**1463–1469.
5. **DeSantis, G., J. Liu, D. P. Clark, A. Heine, I. A. Wilson, and C. H. Wong.** 2003. Structure-based mutagenesis approaches toward expanding the substrate specificity of D-2-deoxyribose-5-phosphate aldolase. Bioorg. Med. Chem. **11:**43–52.
6. **Gijsen, H. J. M., and C. H. Wong.** 1994. Unprecedented asymmetric aldol reactions with three aldehyde substrates catalyzed by 2-deoxyribose-5-phosphate aldolase. J. Am. Chem. Soc. **116:**8422–8423.
7. **Gijsen, H. J. M., and C. H. Wong.** 1995. Sequential three- and four-substrate aldol reactions catalyzed by aldolases. J. Am. Chem. Soc. **117:**7585–7591.
8. **Heine, A., G. DeSantis, J. G. Luz, M. Mitchell, C. H. Wong, and I. A. Wilson.** 2001. Observation of covalent intermediates in an enzyme mechanism at atomic resolution. Science **294:**369–374.
9. **Heine, A., J. G. Luz, C. H. Wong, and I. A. Wilson.** 2004. Analysis of the class I aldolase binding site architecture based on the crystal structure of 2-deoxyribose-5-phosphate aldolase at 0.99 Å resolution. J. Mol. Biol. **343:**1019–1034.

10. **Hennig, M., B. Darimont, R. Sterner, K. Kirschner, and J. N. Jansonius.** 1995. 2.0 Å structure of indole-3-glycerol phosphate synthase from the hyperthermophile *Sulfolobus solfataricus*: possible determinants of protein stability. Structure **3:**1295–1306.
11. **Jennewein, S., M. Schurmann, M. Wolberg, I. Hilker, R. Luiten, M. Wubbolts, and D. Mink.** 2006. Directed evolution of an industrial biocatalyst: 2-deoxy-D-ribose 5-phosphate aldolase. Biotechnol. J. **1:**537–548.
12. **Laskowski, R. A., M. W. MacArthur, D. S. Moss, and J. M. Thornton.** 1993. PROCHECK: a program to check the stereochemical quality of protein structures. J. Appl. Cryst. **26:**283–291.
13. **McRee, D. E.** 1999. XtalView/Xfit: a versatile program for manipulating atomic coordinates and electron density. J. Struct. Biol. **125:**156–165.
14. **Murshudov, G. N., A. A. Vagin, and E. J. Dodson.** 1997. Refinement of macromolecular structures by the maximum-likelihood method. Acta Crystallogr. D **53:**240–255.
15. **Nicholls, A., K. A. Sharp, and B. Honig.** 1991. Protein folding and association: insights from the interfacial and thermodynamic properties of hydrocarbons. Proteins **11:**281–296.
16. **Otwinowski, Z., and W. Minor.** 1997. Processing of X-ray diffraction data collected in oscillation mode. Methods Enzymol. **276:**307–326.
17. **Racker, E.** 1952. Enzymatic synthesis and breakdown of deoxyribose phosphate. J. Biol. Chem. **196:**347–365.
18. **Rashid, N., H. Imanaka, T. Fukui, H. Atomi, and T. Imanaka.** 2004. Presence of a novel phosphopentomutase and a 2-deoxyribose 5-phosphate aldolase reveals a metabolic link between pentoses and central carbon metabolism in the hyperthermophilic archaeon *Thermococcus kodakaraensis*. J. Bacteriol. **186:**4185–4191.
19. **Sakuraba, H., H. Tsuge, I. Shimoya, R. Kawakami, S. Goda, Y. Kawarabayasi, N. Katunuma, H. Ago, M. Miyano, and T. Ohshima.** 2003. The first crystal structure of archaeal aldolase. Unique tetrameric structure of 2-deoxy-D-ribose-5-phosphate aldolase from the hyperthermophilic archaea *Aeropyrum pernix*. J. Biol. Chem. **278:**10799–10806.
20. **Sambrook, J., E. F. Fritsch, and T. Maniatis.** 1989. Molecular cloning: a laboratory manual, 2nd ed. Cold Spring Harbor Laboratory Press, Cold Spring Harbor, NY.
21. **Stura, E. A., S. Ghosh, E. Garcia-Junceda, L. Chen, C. H. Wong, and I. A. Wilson.** 1995. Crystallization and preliminary crystallographic data for class I deoxyribose-5-phosphate aldolase from *Escherichia coli*: an application of reverse screening. Proteins **22:**67–72.
22. **Terwilliger, T.** 2004. SOLVE and RESOLVE: automated structure solution, density modification and model building. J. Synchrotron Radiat. **11:**49–52.
23. **Wong, C. H., E. Garcia-Junceda, L. Chen, O. Blanco, H. J. M. Gijsen, and D. H. Steensma.** 1995. Recombinant 2-deoxyribose-5-phosphate aldolase in organic synthesis: use of sequential two-substrate and three-substrate aldol reactions. J. Am. Chem. Soc. **117:**3333–3339.
24. **Yip, K. S., T. J. Stillman, K. L. Britton, P. J. Artymiuk, P. J. Baker, S. E. Sedelnikova, P. C. Engel, A. Pasquo, R. Chiaraluce, and V. Consalvi.** 1995. The structure of *Pyrococcus furiosus* glutamate dehydrogenase reveals a key role for ion-pair networks in maintaining enzyme stability at extreme temperatures. Structure **3:**1147–1158.